Eur Biophys J (2010) 39:1069–1077
DOI 10.1007/s00249-009-0487-0

ORIGINAL PAPER

Structural implications of mutations assessed by molecular dynamics: $Vpu_{1–32}$ from HIV-1

J. Krüger · Wolfgang B. Fischer

Received: 5 February 2009 / Revised: 7 May 2009 / Accepted: 13 May 2009 / Published online: 9 June 2009

Abstract Structural pore models are generated for $Vpu_{1–32}$WT from HIV-1 as well as for three mutants W23L, S24L and R31V. A computational methodology is employed which samples the whole conformational space of the pentameric assemblies of Vpu. The analysis of the related energy landscape reveals a small set of reasonable pore models, which are thoroughly investigated regarding their structural properties as well as their putative stability under native-like conditions. The models are also discussed in respect of earlier experimental findings about their channel activities. The study proposes functional pores reflecting the experimentally found conductance states of Vpu and its mutants.

Keywords Vpu · HIV-1 · Mutation · Conductance · Membrane protein · Protein assembly

Introduction

Viral replication often relies on auxiliary membrane proteins some of which are known to induce permeabilization of the host cell membrane (Fischer 2005). One of these proteins is Vpu, an 81 amino acid membrane protein encoded by human immunodeficiency virus type 1 (Cohen et al. 1988; Strebel et al. 1988). It has a single transmembrane (TM) topology with a large cytoplasmic domain (Montal 2003). The role of Vpu is many fold and includes the down regulation of CD4 in the endoplasmic reticulum (Chen et al. 1993; Friborg et al. 1995; Margottin et al. 1996; Schubert et al. 1995) by the cytoplasmic domain (Schubert et al. 1996a), the permeabilization of cellular membranes by forming channels or pores (Ewart et al. 1996; Mehnert et al. 2007; Schubert et al. 1996b), and modulation of host cell factors via protein–protein interaction such as TASK channels (Hsu et al. 2004) or BST-2 (Neil et al. 2008; van Damme et al. 2008). There is a large amount of structural data available for Vpu which enables the modeling of the protein and its mechanism of function with computational methods (see Fischer 2003; Fischer and Krüger 2009). The transmembrane domain (TMD) of Vpu is relatively conserved (Fischer 2003) and therefore a potential target for antiviral therapy. Amongst the more than 250 known HIV strains, W23 is completely conserved (www.ebi.ac.uk/swissprot). Adjunct S24 or T24 are found to be conserved more than 90%. If mutations are observed in the range of residues 8–32, including the TMD, they usually involve the exchange of one hydrophobic residue against another. The TM motif of Vpu is helical (Kukol and Arkin 1999; Ma et al. 2002; Wray et al. 1999), and experimental evidence has emerged that it forms pentameric assemblies (Hussain et al. 2007).

The presence of hydrophilic residues within a hydrophobic stretch in a pore is an important requisite for channel activity (Unwin 2005). Vpu has a single serine residue (S24) which is within the TMD, as well as a tryptophan (W23) possibly residing close to the lipid tail ester groups (Krüger and Fischer 2008). An arginine residue (R31) has been identified to be part of the link between the TM helix and the second helix which is floating on the membrane surface (Sramala et al. 2003). In an experimental approach,

Viral membrane proteins, Heidelberg, December 2008.

J. Krüger · W. B. Fischer (✉)
Institute of Biophotonics,
School of Biomedical Science and Engineering,
National Yang-Ming University,
155, Sec. 2, Li-Nong St., Taipei 112, Taiwan
e-mail: wfischer@ym.edu.tw

the role of these amino acids has been evaluated using peptides corresponding to the TMD of Vpu in which W23, S24 and R31 have been replaced by hydrophobic residues (W23L, S24L and R31V) (Mehnert et al. 2008). The respective peptides have been reconstituted into artificial bilayers and their potential to induce channel activity has been measured.

Structural data of these mutations in either full length protein or peptides are lacking. We have recently developed a computational method to screen conformational space in high spatial resolution of proteins forming symmetric assemblies (Krüger and Fischer, submitted). With this method, helical monomers are aligned with their helix axis parallel to a central pore axis. The anticipation is to obtain high quality structural models which can be further used in structure-based drug development. In this study, this methodology is used to achieve structural details about mutated TMDs of Vpu in respect to wild-type (WT) Vpu. All models generated are due to multi-nanosecond molecular dynamics (MD) simulations.

Materials and methods

Ideal helices of Vpu_{1-32}WT (MQPIPIVAIV^{10} ALVVAIIIAI^{20} VVWSIVIIEY^{30} RK), Vpu_{1-32}R31V (MQPIPIVAIV^{10} ALVVAIIIAI^{20} VVWSIVIIEY^{30} ***V***K), Vpu_{1-32}S24L (MQPIPIVAIV^{10} ALVVAIIIAI^{20} VVW***L***IVIIEY^{30} RK), Vpu_{1-32}W23L (MQPIPIVAIV^{10} ALVVAIIIAI^{20} VV***L***SIVIIEY^{30} RK) were generated using MOE software (Molecular operating environment, www.chemcomp.com) and its integrated protein builder with backbone dihedrals of $\phi = -65$ and $\psi = -39$ (Krüger and Fischer 2008). Each helix was embedded into a hydrated POPC bilayer system, by removing overlapping lipid and water molecules. The system was minimized and equilibrated for 1 ns while initial position constraints were stepwise reduced (protein, backbone, C_α). For each of the helices, a 10-ns equilibrium MD simulation followed on systems consisting of the peptide, 122 POPC and 3,650 water molecules with a total of 17,586–17,599 atoms.

The topology for the lipid bilayer [POPC (16:0–18:1 Diester PC, 1-Palmitoyl-2-Oleoyl-*sn*-Glycero-3-Phosphocholine)] were created on the basis of the parameters of Chandrasekhar et al. (2003). The lipid/water system consisting of 128 lipid and 3,655 water molecules, was stepwise minimized, and equilibrated. The stability of the bilayer was confirmed by a 70-ns MD simulation (Krüger and Fischer 2008).

All MD simulations were carried out under GROMACS-3.3.2 (Lindahl et al. 2001; van der Spoel et al. 2005) with the Gromos96 (ffG45a3) force field (Schuler et al. 2001). The temperature of the peptide, lipid and the water molecules were separately coupled to a Berendsen thermostat at 310 K with a coupling time of 0.1 ps. Full isotropic pressure coupling was applied using a Berendsen barostat with a coupling time of 1.0 ps and a compressibility of $4.5e{-}5\ bar^{-1}$. Long range electrostatics were calculated using the particle-mesh Ewald (PME) algorithm with grid dimensions of 0.12 nm and interpolation order 4. Lennard–Jones and short-range Coulomb interactions were cut off at 1.4 and 0.8 nm, respectively.

The starting structure for the assembly is the average structure of a principal component analysis (PCA) over the backbone atoms of the whole 10-ns equilibrium MD simulation. Only 18 residues, the core part from A8 to I26, were used for the assembly. The monomeric helices for the mutations W23L, S24L and R31V were created and equilibrated in the same way.

An assembly method implemented in MOE was used to assemble the pore models. The method was described in detail elsewhere (Krüger and Fischer, submitted).

In brief, the helical monomer backbone is aligned along the *z*-axis, and the coordinate origin set to be located in the middle of the monomer. The absolute rotational orientation is irrelevant for the following steps, but for each dataset the same orientation was used. Five copies of the starting structure were placed in the *xy*-plane in a defined way, concerning interhelical distance, relative rotational angle and tilt towards the *z*-axis, to construct a symmetrical pentameric pore. The helical monomers were considered to move only within the membrane plane, not perpendicular along the *z*-axis. Afterwards, the side chain atoms are reconstructed with a relative orientation considered as the most probable by the integrated rotational library. For each conformer, its potential energy is evaluated according to the united-atom Engh–Huber force field parameters in vacuum, which are implemented in MOE. Each of the four datasets, consists of 343,900 individual conformations, each characterized by distance, angle and tilt, as well as an energy value.

The six residues which were removed at either end prior to assembly were reconstructed to analyze structural aspects of the pore models and to evaluate their stability. Short ideal helices of nine residues in length were aligned with the core part creating an overlap of three residues. The superposition is based on the C_α of these three residues. After removing the overlap, the parts are connected and a brief energy minimization is applied.

The pore models of WT and all mutations were embedded into POPC bilayer (see above) the same way as the monomers. To minimize stress induced by lateral pressure fluctuations, each pore model was simulated with constraints for 1 ns using surface-tension pressure coupling with a tension of 37.5 mN/m. The unconstrained models were submitted to production runs of 50 ns with semi-isotropic pressure coupling applying 1 bar in *z*-direction while

keeping the *xy*-plane fixed. The systems of the pore models consisted of 5 peptides, 112 POPC and 6,453 waters with a total of 26,643–26,708 atoms.

The simulations were run on a DELL Precision 490n workstation, a 28-core Opteron-based compute cluster with Infiniband interconnects and on facilities of the Paderborn Center for Parallel Computing PC^2 (http://wwwcs.uni-paderborn.de/pc2/).

Plots and pictures were made with OriginPro-7.0, VMD-1.8.6 and MOE-2007.09.

Results

Equilibration of monomers

The monomeric peptides of $Vpu_{1–32}$WT and its mutants have been embedded as ideal helix in a fully solvated POPC bilayer and equilibrated for 10 ns using Gromacs-3.3.2 (Lindahl et al. 2001; van der Spoel et al. 2005). The (ideal) helical motif remained intact. As reported earlier, $Vpu_{1–32}$WT develops a bend over the whole length of the membrane spanning part and shows a kink around S23, stabilized by an intramolecular H-bond of its side chain with neighboring backbone carbonyl oxygen (Krüger and Fischer 2008). For the mutations W23L and R31L, this conformation remains the same (Fig. 1). Mutant S24L lacks the ability to form such a hydrogen bond as mentioned for the WT and does not develop any kink or bend, remaining a nearly ideal helix.

The crosswise comparison of the equilibrated averaged monomers derived from a principle component analysis (PCA) shows little deviation between WT and the three mutants (Table 1). The values range from 0.51 to 1.11 Å for the C_α-atoms of the core part (residues 8–26) of the monomers. The smallest deviation of 0.51 Å is found between WT and R31V indicating very similar structures. At the N- and C-termini, partial unwinding has occurred, mainly due to strong interaction of polar/charged residues with the lipid head group. To avoid artificial interactions, only the core portion of each peptide is used for the assembly. The first seven and the last six residues are omitted.

Pore assembly

The assembly of multiple monomers to form a pore structure is carried out with the simulation package MOE. The distance between the monomers, the rotation around their helical axis and the tilt relative to the membrane normal are varied systematically. A major aspect of this approach is to consider homo-oligomers as symmetrical towards their central pore axis. Furthermore, the helical monomers are considered to move only within the membrane plane and not perpendicular to it (along the *z*-axis). These assumptions drastically narrow the search space (Krüger and Fischer, submitted).

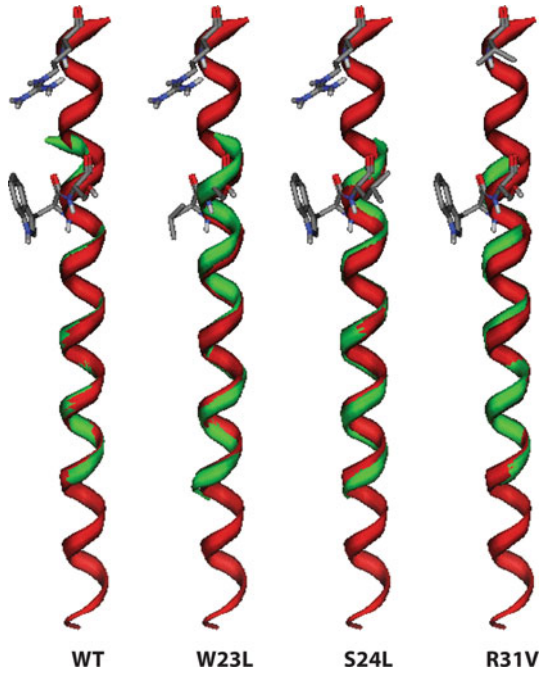

Fig. 1 Superposition of the initially ideal helices with the equilibrated averaged core part derived by PCA each over 10-ns simulation. W23L, S24L and R31V are shown only on the initial ideal helices (*red*), as the assembly is purely based on the backbone of the averaged structures (*green*)

Table 1 RMSD values derived from the cross-wise comparison over all monomers used for the assembly

	WT	W23L	S24L	R31V
WT	–			
W23L	1.00	–		
S24L	0.95	0.98	–	
R31V	0.51	1.11	0.87	–

The values are based on the relative distance of the C_α-atoms of the average PCA structures for residues A8–V26

The energy plots shown in Fig. 2 are two-dimensional projections of the four-dimensional datasets. Minima in the projections represent low energy conformations and neighboring data points reflect structural similarity. But it may happen that two conformations have, e.g., very similar distance and angle values but different tilts. Considering this, five structurally distinct low energy conformations can be identified for $Vpu_{1–32}$WT representing putative open or closed state of the ion conducting pore. For W23L and S24L, six low energy models can be envisaged, and for R31V, four models. The data for WT have been reported elsewhere (Krüger and Fischer, submitted).

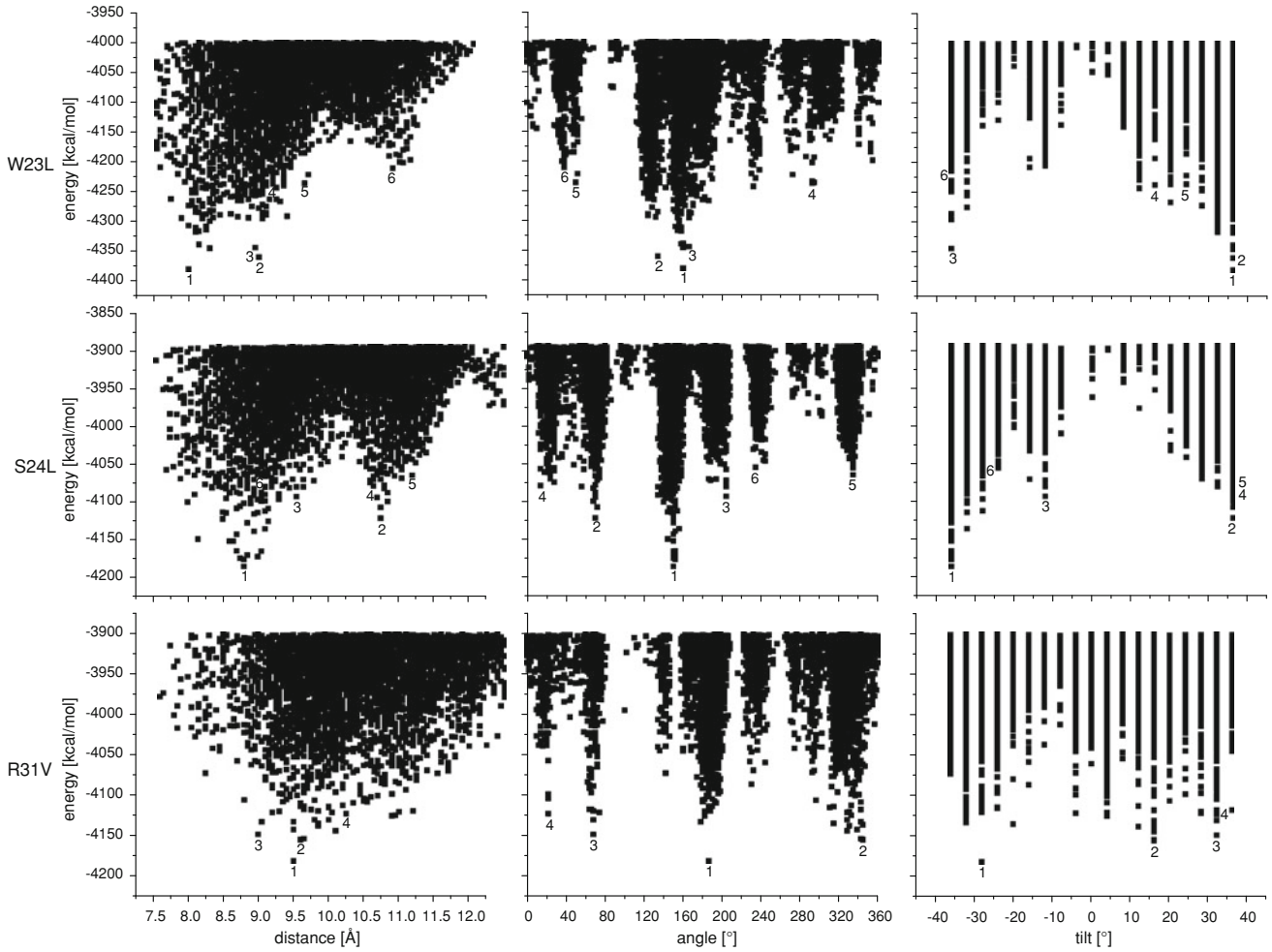

Fig. 2 Energy plots of the assembly of the three mutations W23L, S24L and R31V. Distinct minima in these plots are considered reasonable pore models representative for the cluster of similar conformations around it. Data for the WT are available (Krüger and Fischer, submitted)

Almost identical patterns in the energy landscape can be found between WT and R31V plots. Especially, the occurrence of models with a tilt close to 0° is not observed for W23L and S24L. The main minima on the distance landscape shifts for W23L and S24L by roughly 1 Å compared to the WT to 8.0–9.0 Å. This indicates a significantly tighter packing and a potentially more closed pore. On this landscape a secondary minimum also appears for both W23L and S24L at approximately 10.5 Å, indicating that intermediate distances have become unfavorable through the mutation. Since the rotational angle has no absolute zero, all four Vpu assemblies are oriented in the same way by superposing the monomers prior to assembly. Thus, by enabling comparability, it can be stated that the main minimum between 160° and 200° undergoes some minor shifts but principally remains the same for all mutations.

Structural properties of the pores

Based on the chosen models (Fig. 2, Table 2) and visible inspection, these models can be categorized into three classes depending on the position of the individual residues within the bundle: the orientation of the three mutated residue side chains would face the lumen of the pore ‘in’, the lipid environment ‘out’ or being located between two monomers ’buried’ (Table 2). The categorization into the three classes varies depending on the position of the individual residues along the helix. Analysis from a purely geometrical point of view would allow for the pore models adopting significant tilts up to 32° leading to considerable helix crossing. In such a conformation, R31 can hardly be found ‘buried’, whilst this orientation is likely to be found for W23 and S24.

Table 2 Orientation of mutated side chains for different models of Vpu_{1-32}WT and mutations W23L, S24L and R31V

	Model	W23	S24	R31	Energy (kcal/mol)
WT	1	in	out	out	−4258
	2	out	buried	out	−4201
	3	out	buried	out	−4194
	4	buried	buried	in	−4191
	5	out	out	out	−4182
W23L	1	(out)	buried	out	−4380
	2	(out)	buried	out	−4360
	3	(out)	out	out	−4344
	4	(out)	in	in	−4238
	5	(buried)	buried	in	−4236
	6	(buried)	out	out	−4211
S24L	1	buried	(out)	out	−4185
	2	in	(out)	out	−4122
	3	out	(buried)	out	−4093
	4	in	(buried)	out	−4079
	5	buried	(buried)	out	−4064
	6	out	(buried)	out	−4054
R31V	1	out	buried	(out)	−4182
	2	buried	buried	(out)	−4155
	3	in	out	(out)	−4149
	4	in	out	(out)	−4123

The orientations are categorized into '*in*' facing the lumen of the pore, '*out*' facing the lipid environment or '*buried*' being located at the monomer interface. The entries in parentheses refer to the actual mutation and indicate the orientation of the leucine or valine

The 'out/buried/out' motif is found for 7 out of 25 models for all mutants. This is a considerable number since 27 motifs can theoretically be found.

The energy differences of approximately 100 kcal/mol between the different models for each mutant are too small to favor one model over the other at this stage (Table 2). As the water and lipid molecules were not present during the assembly, their energetic contribution, especially under native conditions, can easily exceed the energy difference observed between the models.

Dynamic properties of the pores

Twenty-one models are individually embedded into a POPC bilayer to study the stability of the models generated. In order to minimize lateral stress due to pressure coupling and rescaling of the simulation box, each model was first simulated with a surface tension of 37.5 mN/m on the surrounding lipid bilayer. The production runs over 50 ns for each of the models were carried out with unconstraint pores and a fixed *x*/*y*-plane, only allowing pressure coupling in the *z*-direction. The C_α root mean square deviation (RMSD) of the individual subunit of each pore is shown in Fig. 3. A strong rise in the RMSD values indicates instability. Even more relevant is the symmetrical behavior of all five subunits of a pore model: if the RMSD for one or two subunits changes while the others remain relative stable, a collapse of the pore occurs.

WT model-2 is considered to be the most stable. WT model-4 also shows leveled RMSD values, except for one subunit (Fig. 3; WT model-4, red curve), indicating an asymmetric deformation of the pore. Consequent MD simulations with this model would eventually lead to a collapse. W23L model-1, model-4 and model-5 show uniformly leveled RMSD curves. S24L model-3, R31V model-1 and model-4 are also stable, with the latter models illustrating that the absolute RMSD value is irrelevant as long as all five subunits retain their symmetry.

The models of the most promising bundle models, including WT are shown in Fig. 4. Whilst WT model-2, W23L model-1 and R31V model-1 adopt a left-handed structure, S24L model-3 adopts a right-handed structure.

Discussion

The conductance and mean open time of an ion-conducting pore is determined by various features of the pore. Besides general aspects like the length of the pore and its diameter, the orientation and polarity of side chains pointing into the lumen of the pore are highly relevant. Polarity or hydrophilicity determines how well a passing ion is stabilized in the narrow part of the pore. The interaction has not to be directly between ion and side chain, the side chain can also interact with the first hydration shell of the ion. The delicate balance between hydrophilic and hydrophobic residues along the path of the ion finally determines the conductance of the pore. Hydrophobic stretches impose a barrier which has to be overcome by the ion. These stretches interrupt the strong interaction of the ion with polar and/or charged side chains which otherwise would trap the ion.

Structural flexibility of the whole pore affects the time-dependent energetic contributions of each of the aforementioned aspects (Portella et al. 2008). A small pore diameter defined by highly flexible side chains could easily show a higher conductance than a wider pore with less flexible side chains. The interaction between the subunits of the pore, as well as the stiffness of each individual subunit, also affects the overall structural flexibility.

Assemblies of the TM part of the Vpu protein show characteristics of an ion channel with a conductance of 16.5 ± 0.09 ps and a mean open time of 496 ± 31.0 ms (Mehnert et al. 2007). It was demonstrated that Vpu is cation selective and that the conductivity for sodium and

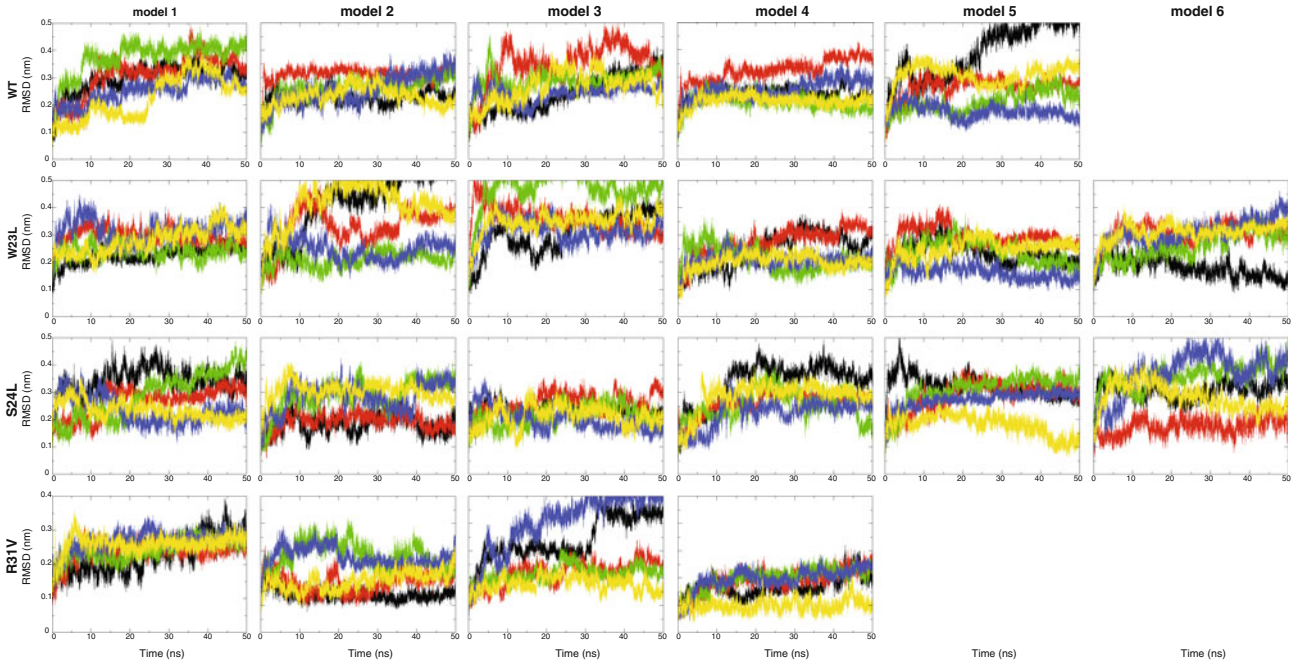

Fig. 3 RMSD plots for all models generated, based on comparison of C_α deviation over 50 ns referring to the starting structure. The values for each monomer of a bundle are shown. WT model-2 is considered stable, while the other models show values for individual monomers changing strongly which results in asymmetric behavior up to complete collapse of the pore, e.g., model-5. For W23L model-1, model-4 and model-5 are stable, as well as model-3 for S24L and model-1 and model-4 for R31V

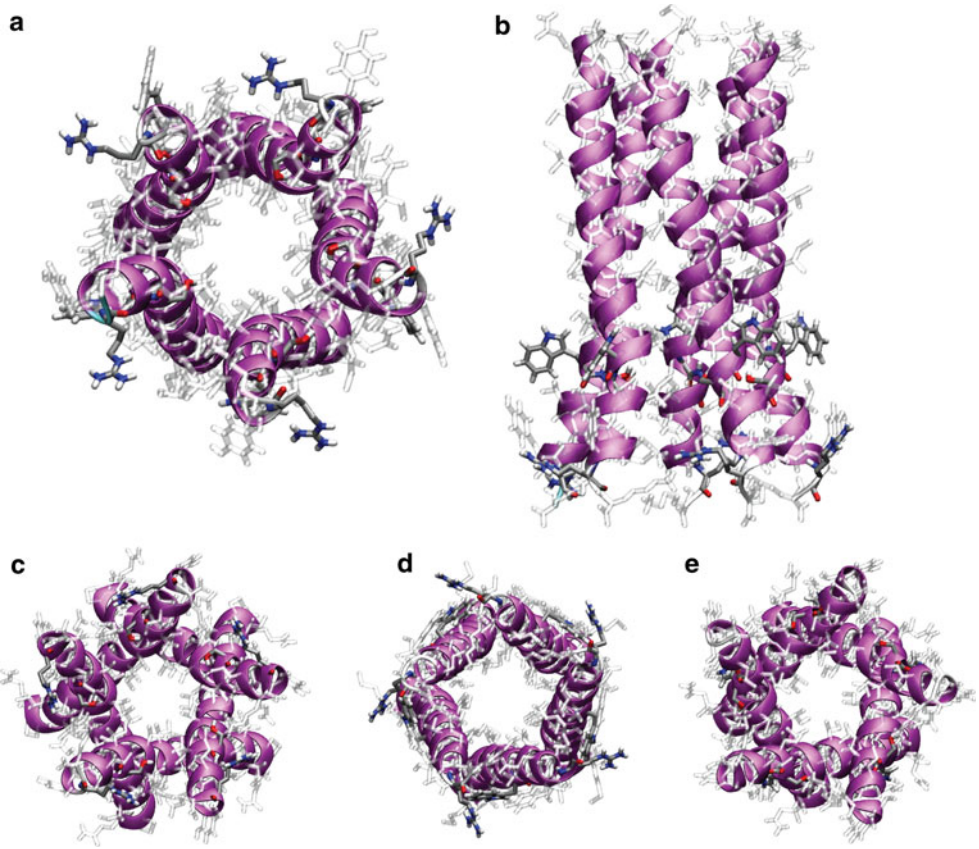

Fig. 4 View along the pore axis (**a**) and from the side (**b**) on model-2 of Vpu_{1-32}WT. The N-termini are pointing to the back (**a**) or upwards (**b**). W23 and R31 are facing out towards the lipid environment while S24 is buried between the subunits. Model-1 of W23L (**c**), model-3 of S24L (**d**) and model-1 of R31V (**e**) are shown in the same orientation as for (**a**). These models are believed to represent the main open conductance state

Table 3 Conductivity data for Vpu_{1-32}WT and mutations derived from experiments (Mehnert et al. 2008)

	Conductance (ps)	Mean open time (ms)
WT	16.5 ± 0.09	496 ± 31.0
W23L	20.6 ± 0.14	795 ± 82.4
S24L	(16.7)	(0)
R31V	17.4 ± 0.28	388 ± 44.5

potassium differs by factor 2. In another study, the properties of the peptides R31V, W23L and S24L have been evaluated (Mehnert et al. 2008). While W23L shows increased conductance and mean open-time, these parameters remain virtually unchanged for R31V compared to the WT. Hardly any channel activity could be observed for S24L indicating that the pore may lack the ability of frequent gating and thus functional pores are difficult to be formed (Table 3).

The experimental data create the opportunity to evaluate how likely a certain side chain orientation of a specific computational model (Table 2) can explain the data. Tryptophan is an aromatic, large and relatively polar residue, which is able to form hydrogen bonds via its NH group. It is unlikely to find this residue buried forming inter-monomer-interactions as its sheer size would impose significant stress on the pore assembly. Similar considerations have to be made if it would face the lumen of the pore. The sheer size of five tryptophans inside the pore would impose a significant obstacle for a passing ion. Furthermore, the NH-groups of the tryptophans would interact with the solvent shell of the ion and trap it. Although this motif is observed for proton-conducting pores like M2 from Influenza A (Nishimura et al. 2002), it is very unlikely that a solvated sodium or potassium could overcome this obstacle (Hub and de Groot 2008). Having the tryptophan facing outwards interacting with the alkyl tails of the surrounding lipid would also not create a perfect interaction. The polar and aromatic side chain would have to align with the lipid tail orientation, also imposing stress on the assembly, as no direct interaction with polar atoms from the lipid head group is possible. Considering the mutation data which show that the conductivity and mean open-time are slightly increased if tryptophan is replaced by leucine, it has to be concluded that the newly introduced side chain is supportive for channel activity. This is best explainable if the mutated residue is oriented outwards, leading to an increased pore radius and higher structural flexibility of the assembly, while not affecting other aspects of the pore.

For the potential orientation of serines only the model with serines pointing outwards can generally considered to be unfavorable. Stabilizing interactions with the permeating ion or its solvent shell would be possible when facing inwards. Such an orientation has also been observed for other ion channels, such as the nicotinic acetylcholine receptor (Unwin 2005). To find serine buried between the subunits also has the potential to be favorable, since intra- and inter-monomeric hydrogen bonds could stabilize pore assembly. In particular, structural effects have occurred which supports the 'buried' orientation of this residue in WT.

The arginine side chain is big but flexible and besides various hydrogen bonding possibilities it is positively charged. Having it pointing inwards would create a voluminous barrier similar to the tryptophan which has to be overcome by the passing ions. An even higher impact on conductance and selectivity would have a conformation which accumulates five arginine side chains around the pore axis. This conformation would lead to repulsion of cations but trapping of anions. A model which has this side chain being 'buried' and interacting with neighboring subunits can be considered reasonable. Also, a model with the arginines pointing outwards would be reasonable, since R31 is found directly at the height of the water/lipid interface (Sramala et al. 2003). R31 anchors the pore well within its lipid environment, interacting with the solvated lipid head groups. Replacing R31 with valine eliminates any interaction with the head groups increasing the structural flexibility of this part of the pore while slightly reducing its stability. This explains the experimental observation of a slightly higher conductance and slightly lower mean open-time compared to the WT.

Following the outlined considerations, one has to conclude that WT model-2 and model-3 fulfil all aspects (Table 2) and therefore they represent a plausible conformation relevant for ion conductivity of Vpu. Both models have similar interhelical distances of 10.05 and 9.40 Å, as well as rotational angles of 192° and 188°. Both models follow the 'out/buried/out' motif. The main difference between the models is due to the tilt of the subunits. For model WT model-2, at tilt of +16° marks a right-handed assembly while WT model-3 is a left-handed assembly with a tilt of −28°.

WT model-5 shows an 'out/out/out' motif and is a potentially closed pore with an interhelical distance of 8.55 Å and tilt and angle of 164° and −4°, respectively. Although it is unlikely that the OH-group of S24 faces the hydrophobic lipid tails directly, S24 can form an internal hydrogen bond, creating a quasi 'buried' state. The low tilt enables a lower interhelical distance and therefore a tighter packing. This conformation can be proposed to be a stable intermediate between WT model-2 and WT model-3 'connecting' them on the high dimensional energy landscape of conformational space.

An open ion-conducting pore has to show some degree of stability and therefore dynamic simulation data are taken into account (Fig. 3). WT model-2 shows reasonable stability

over the 50-ns simulation, while WT model-3 and model-5 show large fluctuations based on the RMSD values. The conductance experiments not only show a closed and open state, but besides the main conductance state they show up to four sub-conductance states. So it may be concluded that WT model-2 represents the main conductance state and WT model-3 or WT model-4 the first sub-conductance states. An unsymmetrical deformation as observed for WT model-5 is not possible for an ion-conducting conformation but may be well suited for a closed state.

The 'out/buried/out' motif is found for WT model-2 and WT model-3, for W23L model-1 and model-2, and S24L model-3 and model-6 as well as for R31V model-1. While all models have rotational orientation between 140° and 220°, their interhelical distance significantly varies between 8.00 and 10.05 Å, as well as the tilt with values between −28° and +36°. It is concluded that conformational transitions between the models occur on the distance and tilt landscapes rather than on the angle landscape. Transitions between open and closed states do most likely only involve small rotational changes.

The data from simulations can also help to identify the ion-conducting conformation for each mutation. W23L model-1 shows the 'out/buried/out' motif and good structural stability, resembling nearly identical rotational angles and tilts as WT model-2 (Fig. 2). The mutation of leucine and its more favorable interaction with lipid tails offers, a conclusive explanation for the increased experimental values (Table 3).

It remains unclear how S24L forms pores in the experiment. Therefore, it is speculative how a computationally derived structural model of an ion-conducting pore looks like. Only S24L model-3 fulfils the 'out/buried/out' criteria. Based on the data presented here, the single helix of S23L lacks a kink and remains straight helical in a lipid bilayer. Taking the left-handed bundle and the experimental data into account, the kink seems to be essential for the proper functioning of the assembly. Its role may be to enable the generation of a small pocket at the C terminus which could harbor a hydrated ion. Structural flexibility gained by the kink could potentially lower the energy barrier for ion permeation.

For R31V, all criteria are only met by model-1, a resemblance of WT model-3. It seems possible that the mutation eliminates 'sub conductance' states.

Conclusion

The extensive search methodology allows assessing structural integrity of bundle models on an atomic level. The search on a large high resolution energy landscape delivers models which remain stable in extended MD simulations.

For Vpu it seems to be essential to adopt a kink within the TMD and possibly a left-handed assembly. Missing these two criteria may still lead to an assembly but may not support channel activity.

The availability of accurate pore models allows the evolvement from sheer assumptions about the effect of point-mutations on the mechanism of function of a protein to reasonable conclusions. The data strongly suggests that WT model-2 (Fig. 2) represents the native main ion-conducting conformation and that transition to sub conductance or closed states mainly involve changes in interhelical distance and tilt.

Acknowledgment WBF acknowledges National Yang-Ming University and the government of Taiwan for financial support (Aim of Excellence Program), as well as the National Science Council of Taiwan (NSC). J.K. acknowledges a fellowship granted jointly by the Alexander von Humboldt-Foundation and NSC. We thank the Paderborn Center for Parallel Computing PC^2 (http://wwwcs.uni-paderborn.de/pc2/) for providing computer time.

References

Chandrasekhar I, Kastenholz M, Lins RD, Oostenbrink C, Schuler LD, van Gunsteren WF (2003) A consistent potential energy parameter set for lipids: dipalmitoyl-phosphatidylcholine as a benchmark of the GROMOS96 45A3 force field. Eur Biophys J 32:67–77

Chen M-Y, Maldarelli F, Martin MA, Strebel K (1993) Human immunodeficiency virus type 1 Vpu protein induces degradation of CD4 in vitro: the cytoplasmic domain contributes to Vpu sensitivity. J Virol 67:3877–3884

Cohen EA, Terwilliger EF, Sodroski JG, Haseltine WA (1988) Identification of a protein encoded by the *vpu* gene of HIV-1. Nature 334:532–534. doi:10.1038/334532a0

Ewart GD, Sutherland T, Gage PW, Cox GB (1996) The Vpu protein of human immunodeficiency virus type 1 forms cation-selective ion channels. J Virol 70:7108–7115

Fischer WB (2003) Vpu from HIV-1 on an atomic scale: experiments and computer simulations. FEBS Lett 552:39–46. doi:10.1016/S0014-5793(03)00782-8

Fischer WB (2005) Viral membrane proteins: structure, function and drug design. In: Atassi MZ (ed) Protein reviews, vol 1. Kluwer Academic/Plenum, New York

Fischer WB, Krüger J (2009) Viral channel forming proteins. Int Rev Cell Mol Biol 275:35–63

Friborg J, Ladha A, Göttlinger H, Haseltine WA, Cohen EA (1995) Functional analysis of the phosphorylation sites on the human immunodeficiency virus type-1 Vpu protein. J Acquir Immune Defic Syndr Hum Retrovirol 8:10–22

Hsu K, Seharaseyon J, Dong P, Bour S, Marbán E (2004) Mutual functional destruction of HIV-1 Vpu and host TASK-1 channel. Mol Cell 14:259–267. doi:10.1016/S1097-2765(04)00183-2

Hub JS, de Groot BL (2008) Mechanism of selectivity in aquaporins and aquaglycoporins. Proc Natl Acad Sci USA 105:1198–1203. doi:10.1073/pnas.0707662104

Hussain A, Das SR, Tanwar C, Jameel S (2007) Oligomerization of the human immunodeficiency virus type I (HIV-1) Vpu protein—a genetic, biochemical and biophysical analysis. Virol J 4:1–11. doi:10.1186/1743-422X-4-81

Krüger J, Fischer WB (2008) Exploring the conformational space of Vpu from HIV-1: a versatile and adaptable protein. J Comput Chem 29:2416–2424. doi:10.1002/jcc.20986

Kukol A, Arkin IT (1999) Vpu transmembrane peptide structure obtained by site-specific fourier transform infrared dichroism and global molecular dynamics searching. Biophys J 77:1594–1601. doi:10.1016/S0006-3495(99)77007-4

Lindahl E, Hess B, Van der Spoel D (2001) GROMACS 3.0: a package for molecular simulation and trajectory analysis. J Mol Model 7:306–317

Ma C, Marassi FM, Jones DH, Straus SK, Bour S, Strebel K, Schubert U, Oblatt-Montal M, Montal M, Opella SJ (2002) Expression, purification, and activities of full-length and truncated versions of the integral membrane protein Vpu from HIV-1. Protein Sci 11:546–557. doi:10.1110/ps.37302

Margottin F, Benichou S, Durand H, Richard V, Liu LX, Benarous R (1996) Interaction between the cytoplasmic domains of HIV-1 Vpu and CD4: role of Vpu residues involved in CD4 interaction and in vitro CD4 degradation. Virology 223:381–386. doi:10.1006/viro.1996.0491

Mehnert T, Lam YH, Judge PJ, Routh A, Fischer D, Watts A, Fischer WB (2007) Towards a mechanism of function of the viral ion channel Vpu from HIV-1. J Biomol Struct Dyn 24:589–596

Mehnert T, Routh A, Judge PJ, Lam YH, Fischer D, Watts A, Fischer WB (2008) Biophysical characterisation of Vpu from HIV-1 suggests a channel-pore dualism. Proteins 70:1488–1497. doi:10.1002/prot.21642

Montal M (2003) Structure–function correlates of Vpu, a membrane protein of HIV-1. FEBS Lett 552:47–53. doi:10.1016/S0014-5793(03)00849-4

Neil SJD, Zang T, Bieniasz PD (2008) Tetherin inhibits retrovirus release and is antagonized by HIV-1 Vpu. Nature 451:425–431. doi:10.1038/nature06553

Nishimura K, Kim S, Zhang L, Cross TA (2002) The closed state of a H^+ channel helical bundle combining precise orientational and distance restraints from solid state NMR. Biochemistry 41:13170–13177. doi:10.1021/bi0262799

Portella G, Hub JS, Vesper MD, De Groot BL (2008) Not only enthalpy: large entropy contribution to ion permeation barriers in single-file channels. Biophys J 95:2275–2282. doi:10.1529/biophysj.108.130609

Schubert U, Clouse KA, Strebel K (1995) Augmentation of virus secretion by the human immunodeficiency virus type 1 Vpu protein is cell type independent and occurs in cultured human primary macrophages and lymphocytes. J Virol 69:7699–7711

Schubert U, Bour S, Ferrer-Montiel AV, Montal M, Maldarelli F, Strebel K (1996a) The two biological activities of human immunodeficiency virus type 1 Vpu protein involve two separable structural domains. J Virol 70:809–819

Schubert U, Ferrer-Montiel AV, Oblatt-Montal M, Henklein P, Strebel K, Montal M (1996b) Identification of an ion channel activity of the Vpu transmembrane domain and its involvement in the regulation of virus release from HIV-1-infected cells. FEBS Lett 398:12–18. doi:10.1016/S0014-5793(96)01146-5

Schuler LD, Daura X, van Gunsteren WF (2001) An improved GROMOS96 force field for aliphatic hydrocarbons in the condensed phase. J Computational Chem 22:1205–1218

Sramala I, Lemaitre V, Faraldo-Gomez JD, Vincent S, Watts A, Fischer WB (2003) Molecular dynamics simulations on the first two helices of Vpu from HIV-1. Biophys J 84:3276–3284. doi:10.1016/S0006-3495(03)70052-6

Strebel K, Klimkait T, Martin MA (1988) Novel gene of HIV-1, *vpu*, and its 16-kilodalton product. Science 241:1221–1223. doi:10.1126/science.3261888

Unwin N (2005) Refined structure of the nicotinic acetylcholine receptor at 4 Å resolution. J Mol Biol 346:967–989. doi:10.1016/j.jmb.2004.12.031

van Damme N, Goff D, Katsura C, Jorgensen RL, Mitchell R, Johnson MC, Stephens EB, Guatelli J (2008) The interferon-induced protein BST-2 restricts HIV-1 release and is downregulated from the cell surface by the viral Vpu protein. Cell Host Microbe 3:1–8. doi:10.1016/j.chom.2007.12.002

van der Spoel D, Lindahl E, Hess B, Groenhof G, Mark AE, Berendsen HJC (2005) Gromacs: fast, flexible and free. J Comput Chem 26:1701–1718. doi:10.1002/jcc.20291

Wray V, Kinder R, Federau T, Henklein P, Bechinger B, Schubert U (1999) Solution structure and orientation of the transmembrane anchor domain of the HIV-1-encoded virus protein U by high resolution and solid-state NMR spectroscopy. Biochemistry 38:5272–5282. doi:10.1021/bi982755c